2021

Simulation-based Study on Predicting the Flow-induced Noise near the Expansion Device

Yingyue Zhang
University of Illinois, yyzhang1995@outlook.com

Stefan Elbel
University of Illinois

Simulation-based Study on Predicting the Flow-induced Noise near the Expansion Device

Yingyue Zhang[1], Stefan Elbel[1,2*]

[1] Air Conditioning and Refrigeration Center
Department of Mechanical Science and Engineering
University of Illinois at Urbana-Champaign
1206 West Green Street, Urbana, IL, 61801, USA
Phone: +1 (217) 819-8603; Email: yingyue2@illinois.edu

[2] Creative Thermal Solutions, Inc.,
2209 North Willow Road, Urbana, IL 61802, USA
Phone: +1 (217) 244-1531; Email: elbel@illinois.edu

* Corresponding Author

ABSTRACT

The flow-induced noise near the expansion device can be very disturbing to users. Studies related to the relationship between the flow-induced noise and flow regimes are calling more and more attention in recent decades. However, current studies lack a quantitative relationship between flow characteristics and the flow-induced noise. Therefore, in this paper, a noise-prediction model is proposed to predict the sound pressure level of flow-induced noise. The paper utilizes a pumped R134a loop with a needle valve for synchronized measurements between flow-induced noise and flow regimes. Synchronized high-speed measurements obtained from a microphone and a high-speed camera enable simultaneous investigation of flow-induced noise and flow regimes. Both the experimental results and the modeling results show that the sound pressure level of gurgling noise increases as the flow quality increases or the system mass flux increases. The relative error of the model for most prediction of flow-induced noise is less than 15%. However, in some high-quality cases, such as annular flow-induced noise, the prediction does not predict the noise well.

1. INTRODUCTION

Most studies in recent years related to the flow-induced noise discussed the qualitative relationship between the flow-induced noise and flow regimes. Han *et al*. in 2011 confirmed that the collapsing bubbles' oscillation frequency equaled the measured flow-induced noise frequency. For instance, the measured frequency of R600a flow-induced noise is about 2 kHz to 4 kHz (Han *et al*., 2011); the measured frequency of R12 flow-induced noise distributes over 4 kHz to 12 kHz (Kim *et al*., 2014). These studies validate that the flow-induced noise is related to the behavior of bubbles near the expansion devices. Hartmann and Melo (2013) found that the condensation-induced shock in the capillary tube causes flow-induced noise in refrigerators. The noise is like popping noise and can be mitigated by installing the internal heat exchanger.

The recent concern about flow-induced noise is the relationship between the flow-induced noise and flow regimes. It is validated that the void fraction at the expansion device inlet influences the generation of flow-induced noise (Tannert and Hesse, 2016). Also, based on experimental data, an empirical R600a flow-induced noise map is generated by Kim *et al*. (2019). The studies related to the flow-induced noise and flow regimes are mostly quantitative. In this paper, a quantitative relationship between the flow characteristics and flow-induce noise is generated. The noise prediction model discussed in the paper is based on the bubble oscillation theory. In the paper, the experimental results using needle valve validate the modeling result of flow-induced noise. The selection of R134a as the refrigerant and needle valve to form the experimental platform should not limit the general applicability of the study's approach and findings to other HVAC&R systems of interest.

2. METHODOLOGY

The flow-induced noise is caused by the oscillations of bubbles near the expansion device. Therefore, the amplitude of flow-induced noise should be related to the bubble number density. The following assumptions are made to establish the noise prediction model related to the bubble oscillation theory:

(1) The vapor at the expansion device outlet will be converted into small bubbles at the expansion device outlet. The total volume of the collapsing bubbles equals the volume of vapor flow at the expansion device inlet. The natural frequency of a spherical bubble is given by equation 1 (Minnaert, 1933):

$$f_{na} = \frac{1}{2\pi r_{eq}} \sqrt{\frac{3\Upsilon P_l}{\rho_l}} \tag{1}$$

In this paper, the polytropic exponent Υ is set as 1.4.

(2) As shown in Figure 1, volume pulsation is the major oscillating behavior of the bubbles. The flow-induced noise generated by the bubble collapse and bubble coalescence is negligible compared to the bubble volume pulsation. All the walls of the bubble move at the same speed during the oscillation process. And all the bubbles passing through the cross-section at a certain point-in-time are assumed to have the same oscillation behavior. The sound pressure radiated by the oscillation of one bubble is shown in equation 2 (Minnaert, 1933):

$$p_s = \frac{3\Upsilon P_l l}{r_{eq}} \tag{2}$$

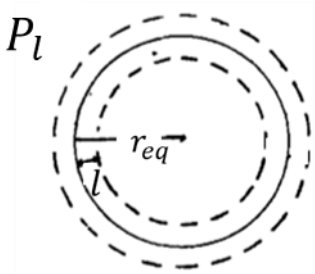

Figure 1. Schematic of bubble volume pulsation (modified from Minnaert, 1933)

(3) The bubble number density is influenced by the void fraction and the bubble size. The definition of bubble number density is shown in equation 3:

$$N_b = \frac{\alpha}{\frac{4}{3}\pi r_{eq}^3} \tag{3}$$

When the bubbles of different sizes appear together, the bubbles increase as the bubble size decreases. The number of bubbles flowing through the cross-section per second can be defined as equation 4:

$$NT = N_b Q_v \tag{4}$$

The period of pressure fluctuation is defined as the inverse of frequency. Within each period, the number of bubbles flowing through the cross-section can be expressed in equation 5:

$$NC = \frac{NT}{f_{na}} \tag{5}$$

(4) The material of the expansion device determines the attenuation effect of the tube wall. The proportion of sound pressure remaining after transmitting through the pipe is shown in equation 6 (Kuhn and Morfey, 1976):

$$\frac{p_{rad}}{p_{int}} = \sqrt{\frac{S_{rad}\rho_l^2 c_l (2\pi f a)^3}{2h^2 E^2}} \tag{6}$$

The sound pressure decreases as the distance increases. The sound pressure at a distance d can be shown in equation 7:

$$p_d = \frac{r_{eq}}{d} p_{int} \tag{7}$$

The relationship between the sound pressure level (SPL) and the sound pressure is given by equation 8:

$$SPL = 20log\ (\frac{p_{RMS}}{p_{ref}}) \quad (8)$$

Where $p_{ref} = 20\mu Pa$, and the $p_{RMS} = \frac{1}{\sqrt{2}}|p_d|$.

3. EXPERIMENTAL SETUP

In this experiment, a pumped loop with R134a is used for circulation, as shown in Figure. 2a. A needle valve is used as a throttling device. The noise measurements are taken in a semi-anechoic chamber. As shown in Figure. 2b, two transparent tubes (1/4 inches) are connected to the needle valve: one is at the needle valve inlet, another is at the needle valve outlet. The hot water loop regulates the quality at the needle valve inlet. By regulating the water mass flow rate and water temperature, the quality of the flow at the TXV inlet varies from 0.05 to 0.5. The mass flux in the system varies from 280 kg m^{-2} s^{-1} to 480 kg m^{-2} s^{-1}. The case conditions are shown in Table 1. A microphone is used to measure the flow-induced noise, and a high-speed camera is used to visualize the flow regimes before and after the needle valve. From Figure. 2c, the high-speed camera is in front of the transparent tube. The microphone is located 2 cm from the needle valve.

The sampling rate of the microphone is set to 44.2 kHz. The human audible zone is from 20 Hz to 20 kHz. The high-speed measurements will cover the range. There are five thermocouples (Type T), two mass flow meters (Micro Motion DX025S and Micro Motion CMF025S), and two pressure transducers (Sensotec TJE) in the experiment. A summary of measured and calculated uncertainties is shown in Table 2.

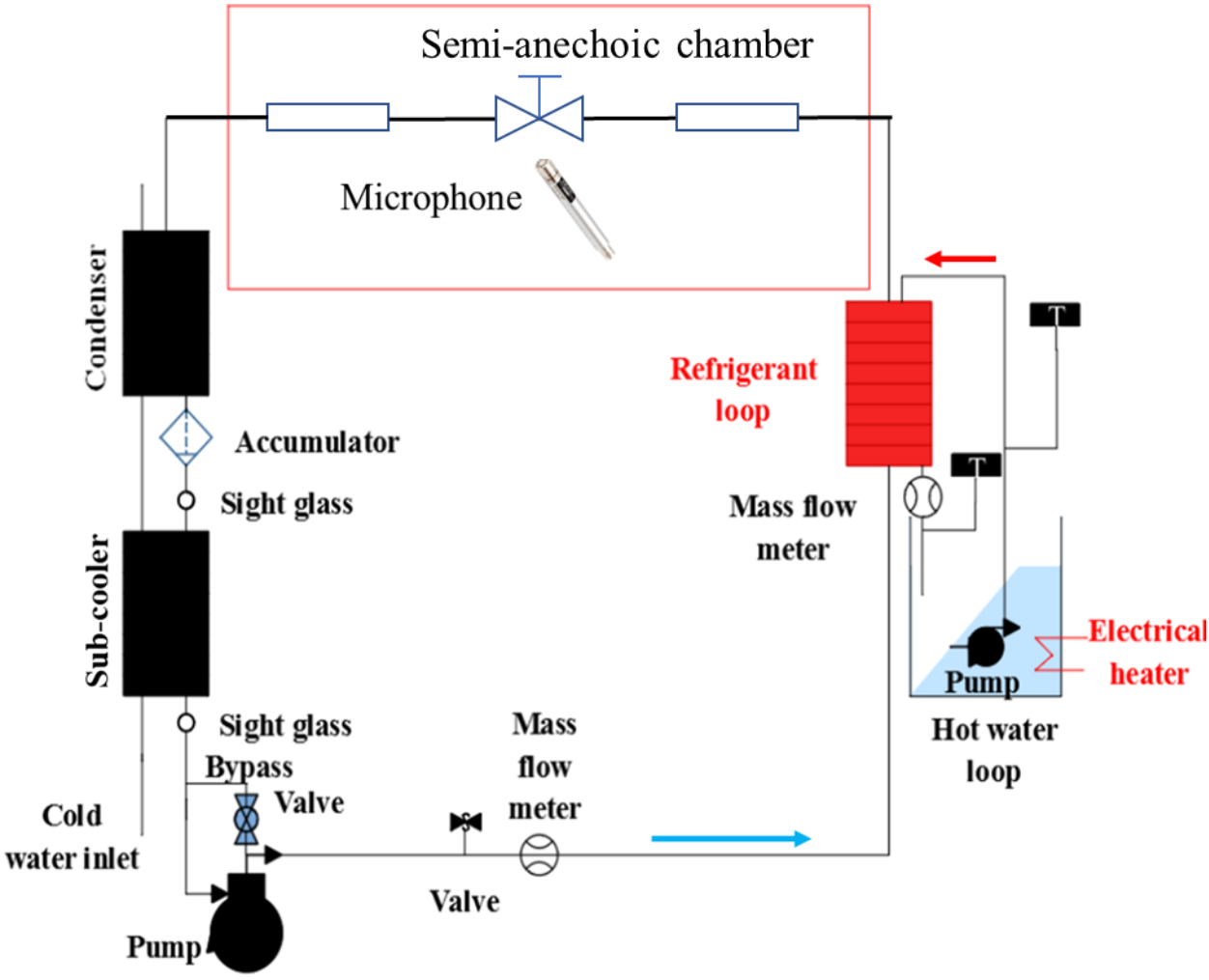

(b) (c)

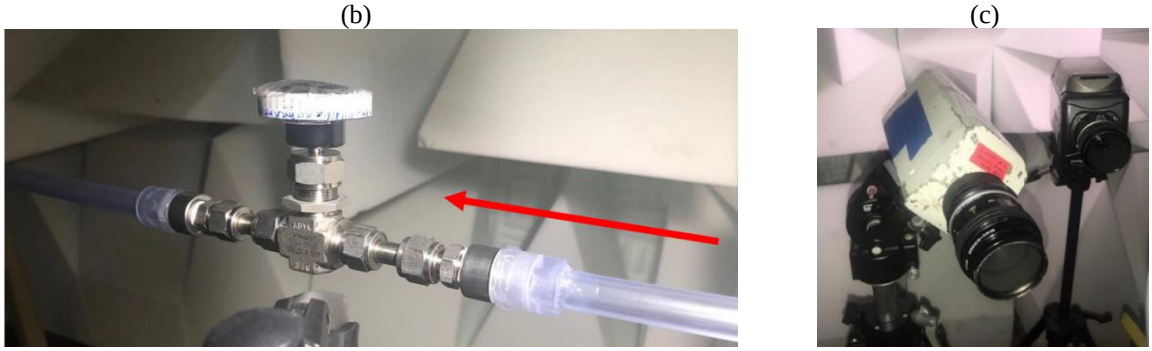

Figure 2. Experimental setup and system schematic (a) system schematic (b) horizontal transparent tubes (c) high-speed cameras (Phantom V4.2)

Table 1. Summary of testing cases

Case number	High-side pressure (kPa)	Low-side pressure (kPa)	Quality (-)	Mass flux (kg m^{-2} s^{-1})
1	831	652	0.2	282
2	777	581	0.3	288
3	694	557	0.4	289
4	645	535	0.5	282
5	802	715	0.05	485
6	839	727	0.05	410
7	908	775	0.05	326

Table 2. Summary of measured and calculated property uncertainties

Thermocouple reading (℃)	Mass flow rate reading (g/s)	Pressure reading (kPa)	Quality (–)
±0.5	±0.1	±7	±0.06

4. RESULTS

From Figure 3, several peaks can be seen in the graph. The peaks appear at around 2 kHz, 7 kHz, 9 kHz, 11 kHz and 13 kHz. The frequency of evaporator flow-induced noise varies from 1 kHz to 4 kHz for different automotive evaporators (Mehendale, *et al*., 2007). Since there is a heat exchanger installed at the needle valve inlet for quality control, the peak near 2 kHz should be flow-induced noise caused by the heat exchanger cavity. Given that the frequency of gurgling noise and hissing noise is known, the model can approximate the bubble size. Since several peaks appear in the spectra, it indicates that bubbles with several different sizes appear at the needle valve outlet. The hissing noise comes from the oscillation of bubbles generated by the cavitation process, while the gurgling noise comes from the oscillation of bubbles collapsing from the vapor flow at the needle valve inlet (Yingyue and Elbel, 2020). The collapsing bubble size usually equals the orifice diameter of the throttling device. It is reasonable to assume that the peak near 6 kHz is the gurgling noise. Other peaks are caused by the oscillation of cavitation bubbles. Therefore, the most obvious peak in the spectra should be the gurgling noise, which is distributed from 5 kHz to 7 kHz. The hissing noise appears from 8 kHz to 13 kHz. The variation of gurgling noise frequency is caused by the variation of the needle position of the valve. Therefore, the void fraction at the needle valve inlet can be used in predicting the gurgling noise. When the needle valve inlet is subcooled, only hissing noise can be heard. The void fraction at the needle valve outlet is used to predict hissing noise. When the needle valve inlet is two-phase, the void fraction used for hissing noise prediction is obtained from the quality difference between the needle valve inlet and needle valve outlet.

As is shown in Figure 3a, the gurgling noise SPL increases as the quality at the needle valve inlet increases. However, when the needle valve inlet's flow quality is 0.5, the flow regime turns to the needle valve inlet's annular flow. The

gurgling noise becomes quieter than the low-quality cases. The modeling results give the same tendency as the experimental results, as shown in Table 3. The prediction of gurgling noise becomes less accurate than when the flow quality at the needle valve inlet increases. As shown in Figure 3b, when the system mass flux increases, the flow-induced noise becomes louder. The tendency is similar in the modeling results. In Figure 4, the relative error for the gurgling noise prediction is shown. It shows that most prediction cases have an error smaller than 10%. When the needle valve inlet is annular flow, the model is not applicable. According to the assumptions, the vapor flow at the needle valve outlet all exists as bubbles. However, for the annular flow, most vapor flow exists as vapor chunks at the outlet. That does not match the assumptions made when establishing the model. It explains the disagreement between the measured annular flow-induced noise and predicted annular flow-induced noise.

(a)

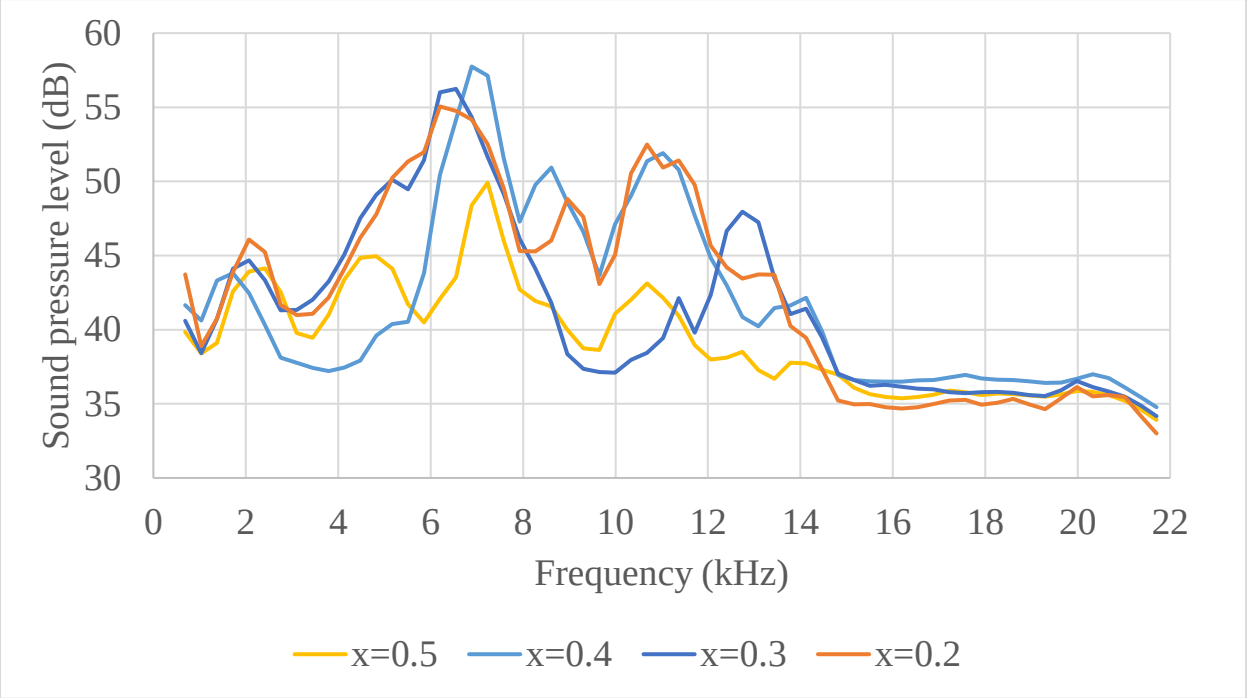

(b)

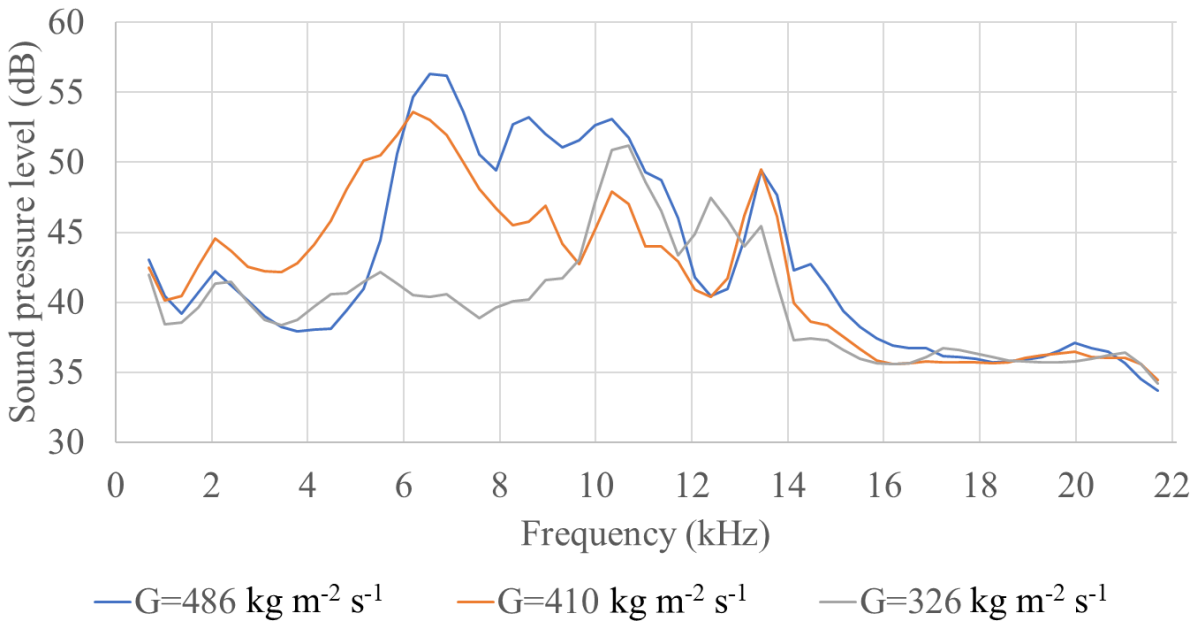

Figure 3. Flow-induced noise spectra comparison (a) different quality at needle valve inlet (G=280 kg m^{-2} s^{-1}) (b) different mass flux (x=0.05)

For the hissing noise prediction, the bubble size distribution can be obtained by equation 3. In this case, the peaks of hissing noise shown in the spectra can be predicted. As shown in Table 4, the prediction of hissing noise is not as accurate as gurgling noise. It shows that the model usually underestimates the hissing noise. The prediction for hissing noise from 12 kHz to 13 kHz is the most accurate. The prediction for other peaks is not close to the real measurements. Most prediction cases for hissing noise have an error smaller than 20%. The possible reason for hissing noise prediction's inaccuracy is that the bubble number density distribution in equation 3 is not for the cavitation process. It can hardly predict the bubble size distribution at the needle valve outlet for the cavitation process. Overall, the hissing noise is harder to predict.

Table 3. Comparison of predicted gurgling noise and measured gurgling noise

Case	Measured SPL of gurgling noise (frequency)	Predicted SPL of gurgling noise (frequency)	Error between measured noise and predicted noise
1	55 dB (5.9 kHz)	53.7 dB (5.9 kHz)	-2.4%
2	56.2 dB (6.2 kHz)	56.4 dB (6.2 kHz)	+0.4%
3	57.7 dB (6.5 kHz)	61 dB (6.5 kHz)	+5.7%
4	50 dB (6.5 kHz)	62.7 dB (6.5 kHz)	+25.4%
5	56.3 dB (6.8 kHz)	52 dB (6.5 kHz)	-7.6%
6	53.6 dB (6.2 kHz)	48.2 dB (6.2 kHz)	-10.1%
7	42.1 dB (5.5 kHz)	42 dB (5.5 kHz)	+0.2%

Table 4. Comparison of predicted hissing noise and measured hissing noise at different frequency

	8 kHz to 9 kHz			10 kHz to 11 kHz			12 kHz to 13 kHz		
Case	Measured noise SPL	Predicted noise SPL	Error	Measured noise SPL	Predicted noise SPL	Error	Measured noise SPL	Predicted noise SPL	Error
1	48.8	45.8	-6.1%	52.5	48.2	-8.2%	No	No	No
2	50	46.7	-6.6%	51	50	-2%	No	No	No
3	No	No	No	42	45	+7.1%	48	46	-4.2%
4	No	No	No	43.1	47.9	+11.1%	No	No	No

5	No	No	No	53	43.8	-17.4%	49.5	47.2	-4.6%
6	47	41.4	-11.9%	47	43.7	-7%	49.5	46.6	-6%
7	51.2	44.9	-12.3%	No	No	No	47.4	46.8	-1.3%

5. CONCLUSIONS

In this paper, a flow-induced noise prediction model is established in the paper. The model is constructed based on the bubble oscillation theory. A pumped R134a system with a needle valve is used to validate the prediction model. The most obvious peak in the spectra should be the gurgling noise, which is distributed from 5 kHz to 7 kHz. The hissing noise appears from 8 kHz to 13 kHz. The flow-induced noise for the needle valve will be louder as the quality and the mass flux increases. The modeling results gives the same tendency as the experimental results. The prediction of gurgling noise is smaller than 10%, except for the annular flow-induced noise. The maximum relative error for hissing noise prediction is about 20%. The prediction for hissing noise is not as good as the gurgling noise prediction is because the bubble number density distribution used in the model does not apply to the cavitation process. Overall, the model gives a quantitative relationship between the flow characteristics and flow-induced noise. The results can help to predict the flow-induced noise when the system conditions are known.

6. REFERENCES

1. Han, H.S., Jeong, W.B., Kim, M.S., 2011. Frequency characteristics of the noise of R600a refrigerant flowing in a pipe with intermittent flow pattern. Int. J. Refrig, 34(6), 1497–1506.
2. Hartmann, D., Melo, C., 2013. Popping noise in household refrigerators: Fundamentals and practical solutions. Appl. Therm. Eng., 51(1-2), 40–47.
3. Kuhn, G.F., Morfey, C.L., 1976. Transmission of low-frequency internal sound through pipe walls. JSV, 47(2), 147-161.
4. Kim, M.S., Jeong, W.B., Han, H.S., 2014. Development of noise pattern map for predicting refrigerant-induced noise. JMST, 28(9), 3499–3510.
5. Kim, G., Lee, J., Park, J., Song, S., 2019. Flow visualization and noise measurement of R410A two-phase flow near electric expansion valve for heating cycle of multi-split air-source heat pump. Appl. Therm. Eng., 157(5), 113712.
6. Minnaert, W.K., 1933. On musical air bubbles and the sound of running water. Philos. Mag., 16(104), 235–248.
7. Tannert, T., Hesse, U., 2016. Noise effects in capillary tubes caused by refrigerant flow. 16th International Refrigeration and Air Conditioning Conference at Purdue, West Lafayette, IN.
8. Zhang, Y. and Elbel, S., 2020. Sound evaluation of flow-Induced noise with simultaneous measurement of flow regimes at TXV inlet of automotive evaporators. SAE Technical Paper 2020-01-1255, 2020.

NOMENCLATURE

Symbols:

a	mean radius of pipe	(m)
A	cross section area	(m^2)
c	sound speed	($m\ s^{-1}$)
d	distance	(m)
E	Young's modulus	(Pa)
f	frequency	(Hz)
g	acceleration of gravity	($m\ s^{-2}$)
G	mass flux	($kg\ m^{-2}\ s^{-1}$)
h	pipe wall thickness	(m)
l	wall distortion	(m)
N	bubble number density	(m^{-3})
NT	number of bubbles flowing through the cross-section	(s^{-1})
NC	number of bubbles per oscillation period	(-)
p	sound pressure	(Pa)
P	pressure	(Pa)
Q	volume flow rate	($m^3\ s^{-1}$)
r	radius	(m)

RMS	root mean square	(-)
S	radiating surface area of pipe	(m^2)
SPL	sound pressure level	(dB)
x	vapor mass fraction (quality)	(-)

Subscripts:

b	bubble
d	distance from the bubble location
eq	equivalent
l	liquid
na	natural frequency
rad	sound power radiated from outer surface
ref	reference
v	vapor

Greek:

Υ	polytropic exponent	(-)
ρ	density	($kg\ m^{-3}$)
α	void fraction	(-)

7. ACKNOWLEDGEMENT

The authors would like to thank the member companies of the Air Conditioning and Refrigeration Center at the University of Illinois at Urbana-Champaign for their financial and technical support and Creative Thermal Solutions, Inc. (CTS) for their technical support.